# NEUTRINO OSCILLATIONS WITH LSND AND MINIBOONE

ION STANCU [a]

*Department of Physics and Astronomy*
*University of Alabama*
*Box 870324*
*Tuscaloosa, AL 35487-0324, USA*
E-mail: ion.stancu@ua.edu

ABSTRACT

A search for $\bar{\nu}_\mu \to \bar{\nu}_e$ oscillations was conducted by the Liquid Scintillator Neutrino Detector (LSND) at the Los Alamos Neutron Science Center (LANSCE) using a $\bar{\nu}_\mu$ beam from $\mu^+$ decay at rest. A total excess of $87.9 \pm 22.4 \pm 6.0$ events cosnsitent with $\bar{\nu}_e p \to e^+ n$ scattering was observed above the expected background. This excess corresponds to an oscillation probability of $(0.264 \pm 0.067 \pm 0.045)\%$, which is consistent with an earlier analysis. In conjunction with other known limits on neutrino oscillations, the LSND data suggest that neutrino oscillations occur in the $0.2 - 10$ eV$^2$/c$^4$ $\Delta m^2$ range, indicating a neutrino mass greater than 0.4 eV/c$^2$. A follow-up experiment, MiniBooNE (Booster Neutrino Experiment), currently under construction at FermiLab, should confirm or dismiss the LSND signal.

## 1. Introduction

In the past years, a considerable number of experiments have searched for neutrino oscillations, where a neutrino of one type (say $\bar{\nu}_\mu$) spontaneously transforms into a neutrino of another type (say $\bar{\nu}_e$). In 1995 the LSND experiment first published data showing candidate events that are consistent with $\bar{\nu}_\mu \to \bar{\nu}_e$ oscillations [3)]. Additional data were reported a year later that provided stronger evidence for neutrino oscillations in this channel [4)]. Further supporting evidence has been provided by the signal in the $\nu_\mu \to \nu_e$ charge-conjugate channel [5)]. The two oscillations searches have completely different neutrino fluxes, backgrounds, and systematics from each other. The data presented here correspond to the entire operation of the detector (1993–1998). During this period the LANSCE accelerator operated for 17 months, delivering a total of 28,896 C of protons on the production target.

## 2. Neutrino Source and Detector

The source of neutrinos for this experiment is the interaction of the intense ($\sim 1$ mA) 798 MeV LANSCE proton beam on the A6 production target, which produces a large number of pions, mostly $\pi^+$. The $\pi^-$ are mainly absorbed and only a small fraction decay to $\mu^-$, which in turn are largely captured. Thus, the resulting neutrino

[a]Representing the LSND and MiniBooNE Collaborations

source is dominantly due to $\pi^+$ decays. About 3.4% of the $\pi^+$ produced in this target decay in flight (DIF) before reaching the water-cooled copper beam stop, generating a $\nu_\mu$ flux with energies up to 250 MeV – illustrated in Fig. 1. The remaining $\pi^+$ stop and decay in the beam dump, producing the decay at rest (DAR) $\bar{\nu}_\mu$ flux through the $\pi^+ \to \mu^+ \nu_\mu$ decay, followed by $\mu^+ \to e^+ \nu_e \bar{\nu}_\mu$, with an endpoint energy of 52.8 MeV – illustrated in the same figure.

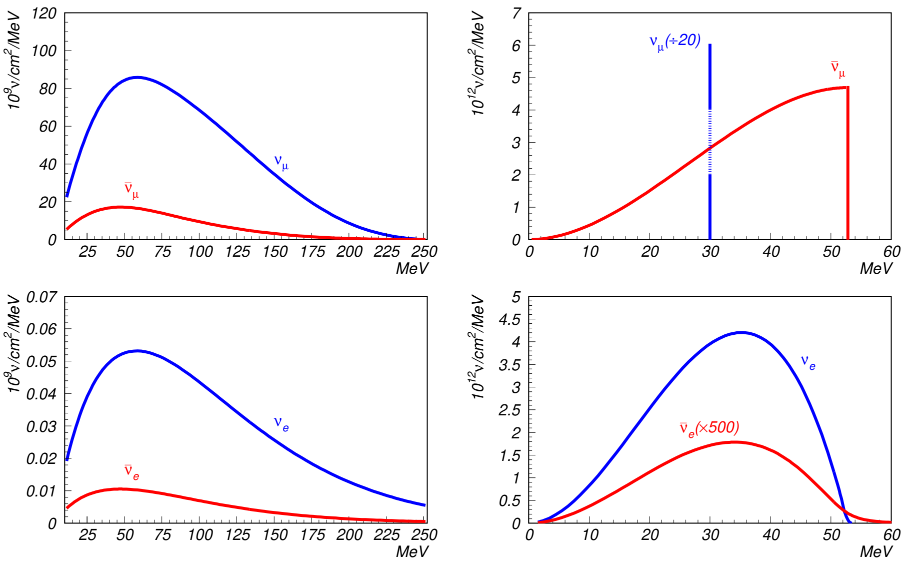


Figure 1: The decay-in-flight (left) and decay-at-rest (right) neutrino fluxes averaged over the LSND detector.

For the 1993–1995 running period the production target consisted of a 30-cm long water target (20-cm in 1993), while for the 1996–1998 running period the production target was reconfigured with the water target replaced by a close-packed, high-Z target. The muon DAR neutrino flux with the latter configuration was only 2/3 of the neutrino flux with the original water target, while the pion DIF neutrino flux was reduced to 1/2 of the original flux. The resulting DAR neutrino fluxes are well understood because almost all detectable neutrinos arise from $\pi^+$ or $\mu^+$ decay; $\pi^-$ and $\mu^-$ that stop are readily captured in the Fe of the shielding and Cu of the beam stop [6]. The production of kaons or heavier mesons is negligible at these proton energies. The $\bar{\nu}_e$ flux is calculated to be only $\sim 8 \times 10^{-4}$ as large as the $\bar{\nu}_\mu$ flux in the $20 < E_\nu < 52.8$ MeV energy range, so that the observation of a $\bar{\nu}_e$ event rate significantly above the calculated background would be evidence for $\bar{\nu}_\mu \to \bar{\nu}_e$ oscillations.

For the first three years of data taking, thin carbon targets were in place in positions A1 and A2 at the experimental area of the LANSCE accelerator, but dominant pion production occurred at the A6 beam stop, which accounted for $\sim 98\%$ of the DAR neutrino flux and $\sim 95\%$ of the DIF neutrino flux. The A1, A2, and A6 targets were approximately 135 m, 110 m, and 30 m, respectively, from the center of the LSND detector. A6 was essentially the only source of neutrinos for the last three years of data taking. Table 1 shows the proton beam statistics for each of the six years of running from 1993 through 1998.

Table 1: Proton beam statistics for each of the years of running (1993–1998).

| Year | Charge (C) | Protons ($\times 10^{22}$) | A6 target | Active Targets |
|---|---|---|---|---|
| 1993 | 1787 | 1.12 | water | A1, A2, A6 |
| 1994 | 5904 | 3.69 | water | A1, A2, A6 |
| 1995 | 7081 | 4.42 | water | A1, A2, A6 |
| 1996 | 3789 | 2.37 | high-Z metal | A6 & partial A2 |
| 1997 | 7181 | 4.48 | high-Z metal | A6 only |
| 1998 | 3154 | 1.97 | high-Z metal | A6 only |

Calculations of $\mu^+$ DAR fluxes are uncertain at the 7% level, while $\pi^\pm$ DIF fluxes and $\mu^-$ DAR fluxes are uncertain to 15% [4]. Neutrino fluxes for the different years of operation are shown in Table 2.

Table 2: Average neutrino fluxes in LSND. Both decay at rest (DAR) and decay in flight (DIF) are shown in $\nu/\mathrm{cm}^2$. The $\nu_\mu$ and $\bar{\nu}_\mu$ DIF fluxes are above the muon production threshold.

| Source | Type | 1993-1995 Flux | 1996-1998 Flux | Total Flux |
|---|---|---|---|---|
| $\mu^+$ DAR | $\bar{\nu}_\mu$ and $\nu_e$ | $7.38 \times 10^{13}$ | $5.18 \times 10^{13}$ | $1.26 \times 10^{14}$ |
| $\mu^-$ DAR | $\nu_\mu$ and $\bar{\nu}_e$ | $5.96 \times 10^{10}$ | $4.87 \times 10^{10}$ | $1.08 \times 10^{11}$ |
| $\pi^+$ DIF | $\nu_\mu$ | $1.37 \times 10^{12}$ | $8.26 \times 10^{11}$ | $2.20 \times 10^{12}$ |
| $\pi^-$ DIF | $\bar{\nu}_\mu$ | $1.45 \times 10^{11}$ | $1.11 \times 10^{11}$ | $2.56 \times 10^{11}$ |
| $\pi^+$ DIF | $\nu_e$ | $5.56 \times 10^{8}$ | $5.01 \times 10^{8}$ | $1.06 \times 10^{9}$ |
| $\mu^+$ DIF | $\nu_e$ | $4.13 \times 10^{9}$ | $2.44 \times 10^{9}$ | $6.57 \times 10^{9}$ |

The LSND detector [7] consisted of an approximately cylindrical tank 8.3 m long by 5.7 m in diameter. On the inside surface of the tank, 1220 8-inch Hamamatsu phototubes (PMTs) covered 25% of the area with photocathode. The tank was filled with 167 metric tons of liquid scintillator consisting of mineral oil and 0.031 g/l of b-PBD. This low scintillator concentration allows the detection of both Čerenkov and scintillation light and yields an attenuation length of more than 20 m for wavelengths greater than 400 nm. PMT time and pulse-height signals were used to reconstruct the track with an average RMS position resolution of $\sim 14$ cm, an angular resolution of $\sim 12$ degrees, and an energy resolution of $\sim 7\%$ at the Michel endpoint of 52.8 MeV. The Čerenkov cone for relativistic particles and the time distribution of the light, which is broader for non-relativistic particles [4], gave excellent separation between electrons and particles below Čerenkov threshold.

A veto shield viewed by 292 5-inch EMI PMTs enclosed the detector on all sides except the bottom. Additional counters were placed below the veto shield after the 1993 run to reduce cosmic-ray background entering through the bottom support structure. The main veto shield [8] consisted of a 15-cm layer of liquid scintillator in an external tank and 15 cm of lead shot in an internal tank. This combination of active and passive shielding tagged cosmic-ray muons that stopped in the lead shot. A veto inefficiency $< 10^{-5}$ was achieved for incident charged particles. Additional passive shielding was provided by about 9 m of Fe-equivalent between the beam stop and the detector, as well as by 2 kg/cm$^2$ of overburden on top of the detector tunnel.

## 3. Neutrino Oscillations Analysis

### *3.1. Primary Electron Selection*

The DAR $\bar{\nu}_e$ candidate events are identified through the inverse $\beta$-decay reaction, $\bar{\nu}_e p \to e^+ n$. Thus, the detection signature consists of a positron and a space-time correlated 2.2 MeV photon, from the neutron capture on free protons ($n\,p \to d\,\gamma$). This two-fold signature provides a unique and powerful $\bar{\nu}_e$ appearance identification and, at the same time, a relatively low level of background – dominated by the intrinsic $\bar{\nu}_e$ contamination in the beam. On the other hand, the DIF $\nu_e$ candidate events are identified through the charged-current reaction $\nu_e C \to e^- X$, i.e., through the detection of an isolated, high-energy electron.

The energy range $20 < E_e < 200$ MeV is chosen so as to accept both DAR $\bar{\nu}_\mu \to \bar{\nu}_e$ and DIF $\nu_\mu \to \nu_e$ oscillation candidates. We require $20 < E_e < 60$ MeV for the $\bar{\nu}_\mu \to \bar{\nu}_e$ oscillation search and $60 < E_e < 200$ MeV for the $\nu_\mu \to \nu_e$ oscillation search. Below 20 MeV there are large backgrounds from the $\beta$ decay of $^{12}B$ created by the capture of stopped cosmic-ray $\mu^-$ on $^{12}C$. Above 200 MeV the beam-related backgrounds from $\pi^+ \to e^+ \nu_e$ are large compared to any likely oscillation signal.

Electron particle identification (PID) for this analysis is achieved through a PID parameter that relies on the quality of the position, timing and angle fit [4]. A new event reconstruction that improved the position resolution and the spatial correlation between the $e^+$ and neutron-capture $\gamma$ in the $\bar{\nu}_e p \to e^+ n$ reaction was applied to the entire 1993–1998 data sample. The previous event reconstruction was limited due to the charge response of the 8-inch PMTs used in LSND (Hamamatsu R1408). For these PMTs, the single photoelectron output charge distribution is approximately a broad Gaussian plus an exponential tail that extends well above the mean of the Gaussian. As the position and angle fits weighted the hit PMTs by their charge, this charge tail has the effect of smearing the reconstructed event positions and angles. To ameliorate this effect, a new reconstruction algorithm was developed that weighted the hit PMTs by a ratio of the predicted charge to the square of the time resolution for that predicted charge, $Q_{pred}/\sigma_t^2$, and not by their measured charge, $Q_{tube}$. This has resulted in an improvement in the position correlation between the muon and the electron from stopped muon decay and between the neutron and the $\gamma$ from neutron capture. The mean reconstructed distance between the muon and decay electron improved from 22 cm with the previous reconstruction to 14 cm with the current reconstruction. For 2.2 MeV $\gamma$ from neutron capture, the most likely distance was reduced from 74 cm to 55 cm. As the accidental $\gamma$ rate is proportional to the cube of this distance, the resulting $\gamma$ reconstruction allows a cut on the $R_\gamma$ parameter (as described below) that yields a factor of two better efficiency with a factor of two reduction in the rate of accidental $\gamma$s.

In addition to a tight electron PID selection, events with a previous activity within 12 $\mu s$, a future activity within 8 $\mu s$, or a bottom veto counter hit were rejected in order to eliminate cosmic-ray muon events. Furthermore, no veto hit is allowed within 30 ns of the trigger time, and the reconstructed electron vertex is required to be inside a volume 35 cm from the faces of the PMTs. Finally, the number of associated $\gamma$s (as defined by the $R_\gamma$ parameter) is required to be $< 2$ ($< 1$) for events $< 60$ ($> 60$) MeV in order to reject neutron-induced events, which tend to have many associated $\gamma$s. Neutrons from $\bar{\nu}_e p \rightarrow e^+ n$ scattering are too low in energy ($< 5$ MeV) to knock out other neutrons; however, higher energy neutrons ($> 20$ MeV) typically knock out one or more neutrons.

The event selection is identical for the DAR and DIF samples except for the associated $\gamma$ criteria. The total efficiency for electrons in the fiducial volume with energies in the range $20 < E_e < 60$ MeV is $0.42 \pm 0.03$.

### *3.2. Correlated 2.2 MeV $\gamma$ Criteria*

Correlated 2.2 MeV $\gamma$ from neutron capture are distinguished from accidental $\gamma$ from radioactivity by use of the likelihood ratio, $R_\gamma$, which is defined to be the likelihood that the $\gamma$ is correlated divided by the likelihood that the $\gamma$ is accidental. $R_\gamma$ depends on three quantities: the number of hit PMTs associated with the $\gamma$ (which is proportional to the $\gamma$ energy), the distance between the reconstructed $\gamma$ position and $e^+$position, and the time between the $\gamma$ and $e^+$ (neutrons have a capture time in mineral oil of 186 $\mu$s, while the accidental $\gamma$ are uniform in time). Figure 2 shows these distributions, which are obtained from fits to the data, for both correlated 2.2 MeV $\gamma$ (solid curves) and accidental $\gamma$ (dashed curves). To determine $R_\gamma$, the product of probabilities for the correlated distributions is formed and divided by the product of probabilities for the uncorrelated distributions. The accidental $\gamma$ efficiencies are measured from the laser-induced calibration events, while the correlated $\gamma$ efficiencies are determined from the Monte Carlo simulation of the experiment. Similar results for the correlated $\gamma$ efficiencies are obtained from cosmic-ray neutron events, whose high energy gives them a slightly broader position distribution. Note that with the new reconstruction, the correlated $\gamma$ efficiency has increased while the accidental $\gamma$ efficiency has decreased. For $R_\gamma > 10$, the correlated and accidental efficiencies are

0.39 and 0.003, respectively. For the previous reconstruction [4] the $R_\gamma^{old} > 30$ cut gave correlated and accidental efficiencies of 0.23 and 0.006, respectively.

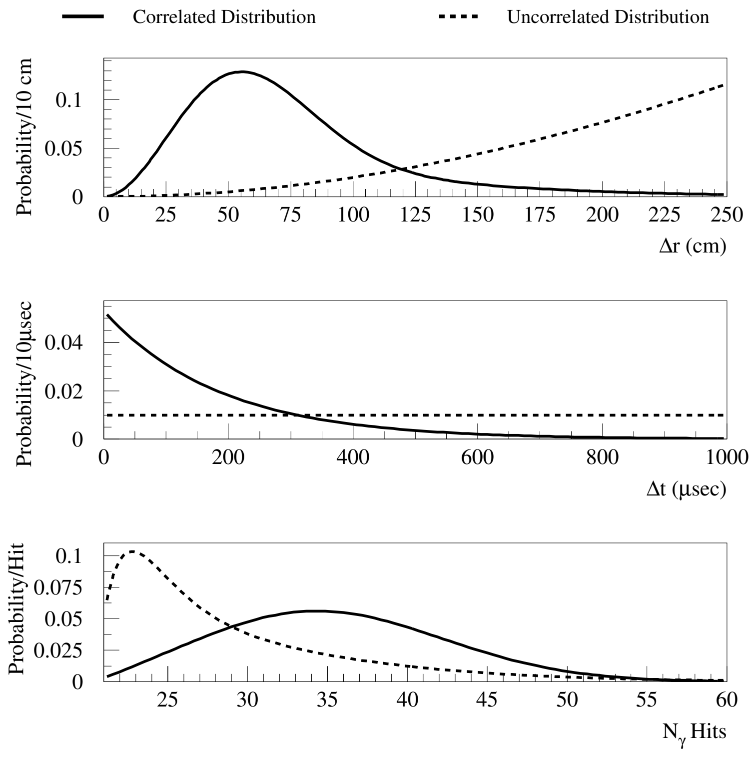


Figure 2: Distributions for correlated 2.2 MeV $\gamma$ (solid curves) and accidental $\gamma$ (dashed curves). The top plot shows the distance between the reconstructed $\gamma$ position and positron position, $\Delta r$, the middle plot shows the time interval between the $\gamma$ and positron, $\Delta t$, and the bottom plot shows the number of hit phototubes associated with the $\gamma$, $N_{hits}$.

As checks of the $R_\gamma$ distributions, several well-known reactions have been examined. By definition, the exclusive $\nu_e C \to e^- N_{gs}$ reaction has no recoil neutron, so that its $R_\gamma$ distribution should be consistent with a purely accidental $\gamma$ distribution [9]. A fit to the $R_\gamma$ distribution finds that the fraction of events with a correlated $\gamma$, $f_c$, is $f_c = -0.004 \pm 0.007$ ($\chi^2 = 4.6/9$ DOF). On the other hand, the sample of $\mu^\pm$ events arising from the reactions $\nu_\mu C \to \mu^- X$, $\bar{\nu}_\mu C \to \mu^+ X$, and $\bar{\nu}_\mu p \to \mu^+ n$ is expected to have $\sim 14\%$ of the events with a correlated $\gamma$ [10]. A fit to the $R_\gamma$ distribution gives $f_c = 0.129 \pm 0.013$ ($\chi^2 = 8.2/9$ DOF), in agreement with expectations.

### *3.3. Neutrino Oscillation Results*

Table 3 shows the statistics for events that satisfy the selection criteria for the primary $\bar{\nu}_\mu \to \bar{\nu}_e$ oscillation search. An excess of events is observed over that expected from beam-off and neutrino background that is consistent with neutrino oscillations. A $\chi^2$ fit to the $R_\gamma$ distribution, as shown in Fig. 3, gives $f_c = 0.0567 \pm 0.0108$

Table 3: Numbers of beam-on events that satisfy the selection criteria for the primary $\bar{\nu}_\mu \rightarrow \bar{\nu}_e$ oscillation search with $R_\gamma > 1$, $R_\gamma > 10$, and $R_\gamma > 100$. Also shown are the beam-off background, the estimated neutrino background, the excess of events that is consistent with neutrino oscillations, and the probability that the excess is due to a statistical fluctuation.

| Selection | Beam-On Events | Beam-Off Background | Beam-Related Background | Event Excess | Probability |
|---|---|---|---|---|---|
| $R_\gamma > 1$ | 205 | $106.8 \pm 2.5$ | $39.2 \pm 3.1$ | $59.0 \pm 14.5 \pm 3.1$ | $7.8 \times 10^{-6}$ |
| $R_\gamma > 10$ | 86 | $36.9 \pm 1.5$ | $16.9 \pm 2.3$ | $32.2 \pm 9.4 \pm 2.3$ | $1.1 \times 10^{-4}$ |
| $R_\gamma > 100$ | 27 | $8.3 \pm 0.7$ | $5.4 \pm 1.0$ | $13.3 \pm 5.2 \pm 1.0$ | $1.8 \times 10^{-3}$ |

($\chi^2 = 10.7/9$ DOF), which leads to a beam on-off excess of $117.9 \pm 22.4$ events with a correlated neutron. Subtracting the neutrino background from $\mu^-$ DAR followed by $\bar{\nu}_e p \rightarrow e^+ n$ scattering ($19.5 \pm 3.9$ events) and $\pi^-$ DIF followed by $\bar{\nu}_\mu p \rightarrow \mu^+ n$ scattering ($10.5 \pm 4.6$ events) leads to a total excess of $87.9 \pm 22.4 \pm 6.0$ events. This excess corresponds to an oscillation probability of $(0.264 \pm 0.067 \pm 0.045)\%$,

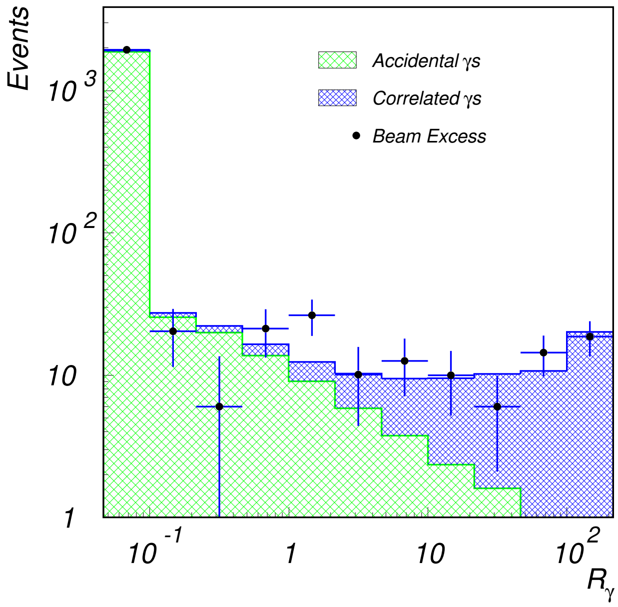


Figure 3: The $R_\gamma$ distribution for events that satisfy the selection criteria for the primary $\bar{\nu}_\mu \rightarrow \bar{\nu}_e$ oscillation search.

where the first error is statistical and the second error is the systematic error arising from uncertainties in the backgrounds, neutrino flux (7%), $e^+$ efficiency (7%), and $\gamma$

efficiency (7%). Note that our previously published result [4)], based on the 1993–1995 data sample, was $(0.31 \pm 0.12 \pm 0.05)\%$.

A clean sample of oscillation candidate events can be obtained by requiring $R_\gamma > 10$, where as shown in Table 3, the beam on-off excess is $49.1 \pm 9.4$ events while the estimated neutrino background is only $16.9 \pm 2.3$ events. Figure 4 displays the energy distribution of these events. The shaded regions show the combination of neutrino background plus neutrino oscillations at low $\Delta m^2$. The data agree well with the oscillation hypothesis.

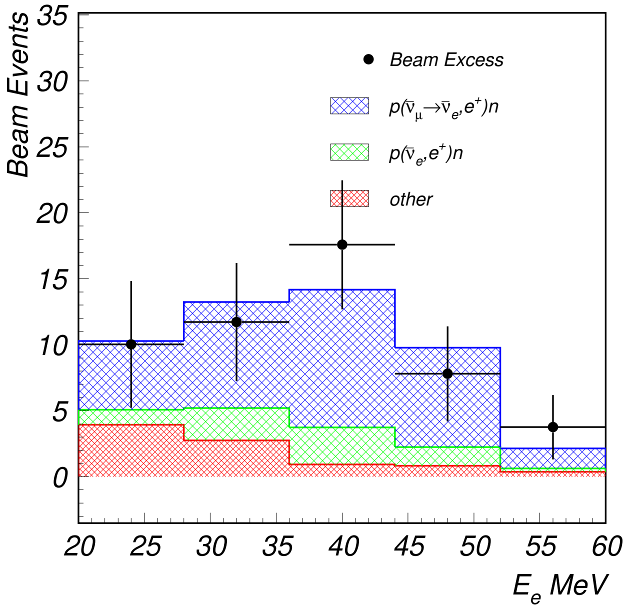


Figure 4: The energy distribution of the 1993–1998 data sample for events with $R_\gamma > 10$. The shaded region shows the expected distribution from a combination of neutrino background plus neutrino oscillations at low $\Delta m^2$.

The neutrino oscillations analysis has been extended up to 200 MeV because there is additional information available and because the DIF data constrains the region $\Delta m^2 > 2$ eV$^2$/c$^4$, even though the event selection was optimized for the DAR energy range and the beam-off backgrounds above 60 MeV are large when using the same selection criteria over the entire energy range. Applying the above analysis to the $60 < E_e < 200$ MeV data sample (except for no associated $\gamma$), involving secondary $\nu_\mu \rightarrow \nu_e$ oscillations only, results in a beam on-off excess of $14.7 \pm 12.2$ events. The signal expected for 100% $\nu_\mu \rightarrow \nu_e$ transmutation is estimated to be 7800 events, and the $\nu_e$ background from $\mu^+ \rightarrow e^+ \bar{\nu}_\mu \nu_e$, $\pi^+ \rightarrow e^+ \nu_e$, and $\nu e \rightarrow \nu e$ is estimated to be $6.6 \pm 1.7$ events, resulting in a total excess of $8.1 \pm 12.2 \pm 1.7$ events or an oscillation probability of $(0.10 \pm 0.16 \pm 0.04)\%$. This result is lower than but consistent with our higher precision analysis of the 1993–1995 data sample [5)], which determined the selection parameters by maximizing the acceptance divided by the square root of the beam-off background and which had much less beam-off background overall.

A $(\sin^2 2\theta, \Delta m^2)$ oscillation parameter fit for the entire data sample ($20 < E_e < 200$ MeV) has been performed, based on the distribution of four variables: the electron energy, $E_e$, the electron reconstructed distance along the tank axis, $z$, the reconstructed direction cosine the electron makes with the incident neutrino, $\cos\theta_\nu$, and the likelihood ratio that the event has a correlated 2.2 MeV $\gamma$, $R_\gamma$. The result of the fit, which is shown in Fig. 5 includes both $\bar{\nu}_\mu \to \bar{\nu}_e$ and $\nu_\mu \to \nu_e$ oscillations, as well as all known neutrino backgrounds. The inner and outer regions correspond to 90%

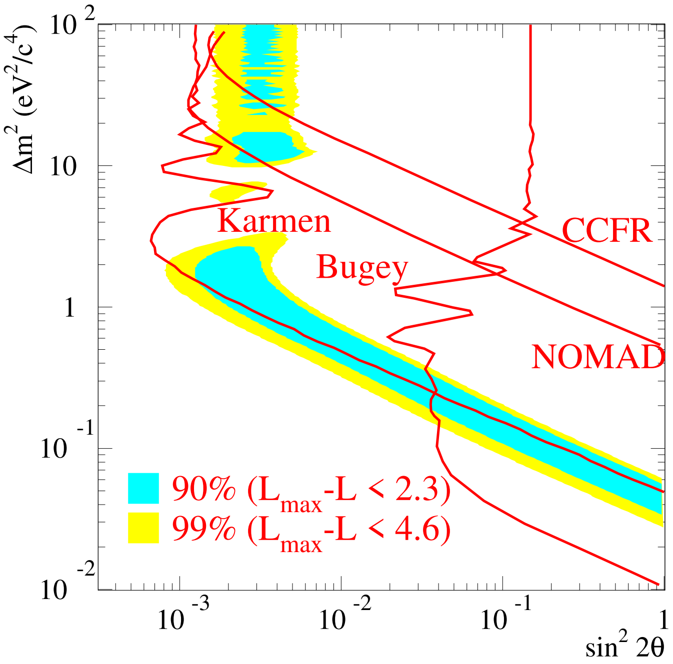


Figure 5: A $(\sin^2 2\theta, \Delta m^2)$ oscillation parameter fit for the entire data sample, $20 < E_e < 200$ MeV. The fit includes primary $\bar{\nu}_\mu \to \bar{\nu}_e$ oscillations and secondary $\nu_\mu \to \nu_e$ oscillations, as well as all known neutrino backgrounds. The inner and outer regions correspond to 90% and 99% CL allowed regions, while the curves are 90% CL exclusion limits.

and 99% CL allowed regions, while the curves are 90% CL limits from the Bugey reactor experiment [11)], the CCFR experiment at Fermilab [12)], the NOMAD experiment at CERN [13)], and the KARMEN experiment at ISIS [14)]. The most favored allowed region is the band from 0.2–2.0 eV$^2$/c$^4$, although a region around 7 eV$^2$/c$^4$ is also possible, but has been made less probable by the $\nu_\mu \to \nu_e$ analysis. The best-fit point is calculated to be $(\sin^2 2\theta, \Delta m^2)_{best-fit} = (0.003, 1.2\ \mathrm{eV}^2/\mathrm{c}^4)$. The number of $\bar{\nu}_\mu \to \bar{\nu}_e$ oscillation events at the best-fit point is 89.5 events, which agrees well with the $87.9 \pm 22.4 \pm 6.0$ event excess from the fit to the $R_\gamma$ distribution. The entire low $\Delta m^2$ region gives an almost equally good fit within 0.5 log-likelihood units.

## 4. MiniBooNE

The Booster Neutrino Experiment (BooNE) at FermiLab consists of a two-detector setup, using a new neutrino beam-line coming off of the FNAL 8 GeV proton booster. The booster is expected to provide $2 \times 10^7$ s of running per year, while delivering $5 \times 10^{12}$ protons per 1 $\mu$s pulse at a rate of 5 Hz to the BooNE detectors, in parallel to supplying protons for the TeVatron and NuMI programs. The secondary pions beam will emerge from a two-horn focusing system into a 50 m decay region. The pion decay length will be either 25 m or 50 m, depending on the position of a movable steel beam stop. This variation in the decay length will provide an important check on the systematics errors for neutrino oscillations.

The first phase of BooNE – MiniBooNE – consists of a single 12-m diameter spherical imaging Čerenkov detector, as shown in Fig. 6, positioned at 500 m downstream from the decay region. The tank is filled with 769 tons of pure mineral oil. The

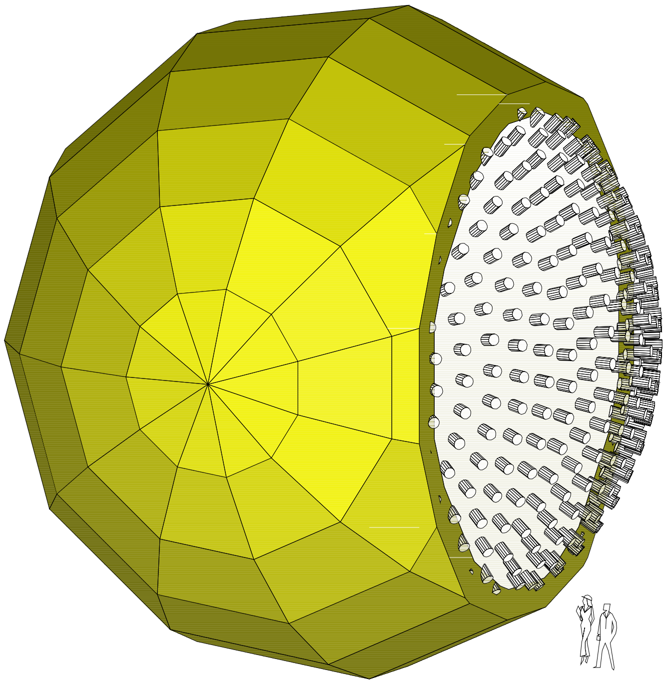

Figure 6: The MiniBooNE detector.

outer volume of the tank is optically isolated from the main volume and serves as an active veto shield for partially contained events and cosmic rays. It is viewed by 240 of the original LSND 8-inch PMTs. The inner volume of the tank is viewed by 1280

8-inch PMTs which provide approximately 11% photo-cathode coverage. 950 of these PMTs are from the now decommissioned LSND experiment, while the remaining 330 of them are newly acquired PMTs, with much better timing and charge resolution.

Typical $\nu_\mu$ energies will be from 0.5 to 1.0 GeV. In one year of running, the experiment will collect approximately 500,000 reconstructed $\nu_\mu C \rightarrow \mu^- X$ events. The intrinsic $\nu_e$ contamination in the beam will be approximately 0.3%, or approximately 1500 reconstructed $\nu_e C \rightarrow e^- X$ background events.

The detector will reconstruct quasi-elastic $\nu_e C \rightarrow e^- X$ interactions (the signature for the $\nu_\mu \rightarrow \nu_e$ appearance) by identifying the electrons via their characteristic Čerenkov and scintillation light signatures. The primary background sources will be due to the intrinsic $\nu_e$ contamination of the beam – due to decays of pions and kaons – as well as from the misidentification of muons and neutral pions in the tank.

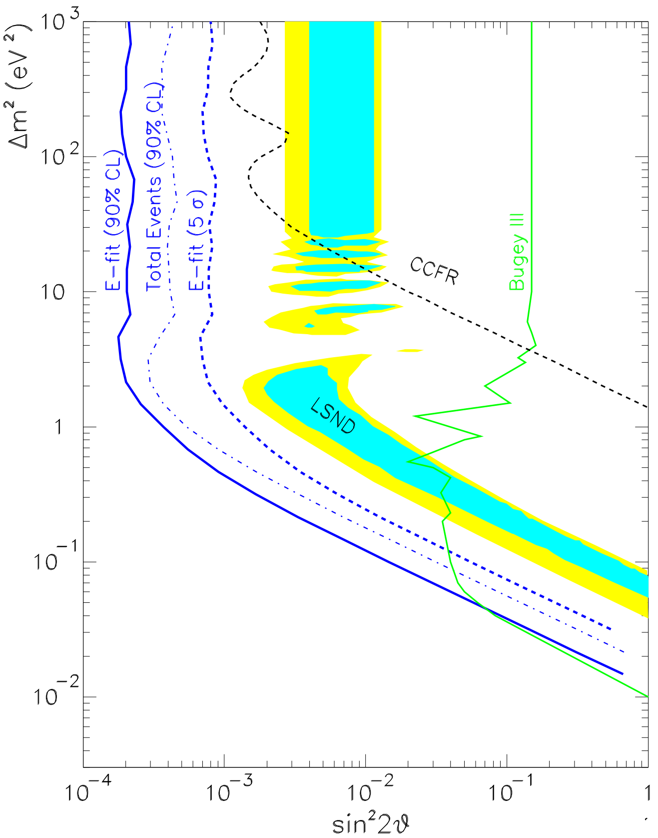


Figure 7: Electron neutrino appearance limits in MiniBooNE.

The MiniBooNE sensitivity to neutrino oscillations is illustrated in Fig. 7. This figure assumes $5 \times 10^{20}$ protons on target, corresponding to approximately one year of running. The 90% confidence sensitivity limits are shown for two analysis techniques: (a) energy fit (solid line), or (b) event counting (dot-dashed line). For large values of $\Delta m^2$ the MiniBooNE experiment covers $\sin^2 2\theta > 3.8 \times 10^{-4}$, and for maximum mixing ($\sin^2 2\theta = 1$) the $\Delta m^2$ coverage extends down to 0.02 eV$^2$. Therefore, if neutrino oscillations occur indeed as indicated by LSND, MiniBooNE should be able to observe a well-defined $\nu_e$ event excess after only one year of operation. Figure 8 shows the number of excess events and their significance for two points in the LSND favoured region.

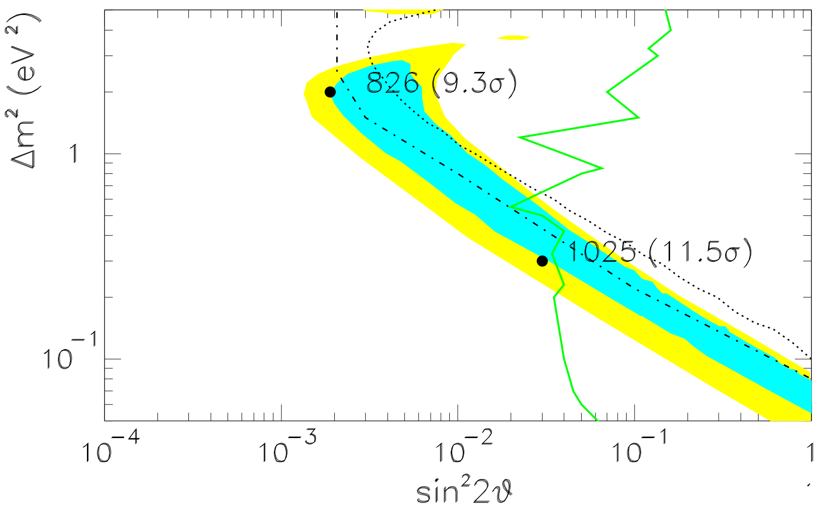


Figure 8: The expected number of excess events in MiniBooNE and their significance for two points in the LSND decay-at-rest allowed region, after one year of data collection.

The MiniBooNE detector and the new 8 GeV neutrino beam line are currently under construction at FermiLab, and the experiment is scheduled to start data taking early 2002. Should there be an unambiguous oscillation signal, the second phase of the experiment would proceed placing a second identical detector at about 1000 m from the decay region. The full BooNE setup will then be able to make high precision measurements of the neutrino oscillation parameters that govern the $\nu_\mu \to \nu_e$ transitions.

## 5. Conclusions

The LSND experiment provides evidence for neutrino oscillations from the primary $\bar{\nu}_\mu \to \bar{\nu}_e$ oscillation search. A total excess of $87.9 \pm 22.4 \pm 6.0$ $\bar{\nu}_e p \to e^+ n$ events with $e^+$ energy between 20 and 60 MeV is observed above expected neutrino-induced backgrounds. This excess corresponds to an oscillation probability of $(0.264 \pm 0.067 \pm 0.045)\%$. A fit to all of the LSND neutrino processes determines the allowed oscillation parameters in a two–generation model. In conjunction with other available neutrino oscillation limits, the LSND data suggest that neutrino flavor oscillations occur with a $\Delta m^2$ in the range 0.2-10 eV$^2$/c$^4$. At present, this remains the only evidence for appearance neutrino oscillations and implies that at least one neutrino has a mass greater than 0.4 eV/c$^2$. The MiniBooNE experiment at Fermilab, which is presently under construction, is expected to provide a definitive test of the LSND results, and if the neutrino oscillation results are confirmed, will make a precision measurement of the oscillation parameters.

## 6. References


1) The LSND collaboration consists of: I. Stancu (University of Alabama); E. D. Church, G. J. VanDalen (UC Riverside); W. Vernon (UC San Diego); D. O. Caldwell, S. Yellin (UC Santa Barbara); D. Smith (Embry Riddle Aeronautical University); R. Tayloe (Indiana University); A. Aguilar, R. L. Burman, J. B. Donahue, G. T. Garvey, W. C. Louis, G. B. Mills, V. Sandberg, D. H. White (Los Alamos National Laboratory); R. Imlay, A. Malik, W. Metcalf, M. Sung, N. Wadia (Louisiana State University); A. K. Cochran, A. Fazely, R. Gunasingha (Southern University); L. B. Auerbach, R. Majkic (Temple University).
2) The MiniBooNE collaboration consists of: I. Stancu (University of Alabama); S. Koutsoliotas (Bucknell University); E. D. Church, G. J. VanDalen (UC Riverside); R. A. Johnson, J. L. Raaf, N. Suwonjandee (University of Cincinnatti); L. Bugel, J. M. Conrad, B. T. Fleming, J. Formaggio, M. H. Shaevitz, M. Sorel, E. D. Zimmerman (Columbia University); D. Smith (Embry Riddle Aeronautical University); C. Bhat, S. Brice, B. C. Brown, R. Ford, F. G. Garcia, P. Kasper, T. Kobilarcik, I. Kourbanis, A. Malensek, W. Marsh, P. Martin, F. Mills, C. Moore, P. Nienaber, A. Russell, P. Spentzouris, R. Stefanski, T. Williams (Fermi National Accelerator Laboratory); R. Tayloe (Indiana University); G. T. Garvey, E. Hawker, W. C. Louis, G. B. Mills, V. Sandberg, B. Sapp, R. Schirato, D. H. White (Los Alamos National Laboratory); R. Imlay, W. Metcalf, M. Sung (Louisiana State University); B. P. Roe (University of Michigan); A. O. Bazarko, P. D. Meyers, F. C. Shoemaker (Princeton University).
3) C. Athanassopoulos, *et al.*, Phys. Rev. Lett. **75**, 2650 (1995).
4) C. Athanassopoulos, *et. al.*, Phys. Rev. C **54**, 2685 (1996); Phys. Rev. Lett. **77**, 3082 (1996).
5) C. Athanassopoulos, *et al.*, Phys. Rev. C **58**, 2489 (1998); Phys. Rev. Lett. **81**, 1774 (1998).
6) R. L. Burman, M. E. Potter, and E. S. Smith, Nucl. Instrum. Methods A **291**, 621 (1990); R. L. Burman, A. C. Dodd, and P. Plischke, Nucl. Instrum. Methods A **368**, 416 (1996).
7) C. Athanassopoulos, *et al.*, Nucl. Instrum. Methods A **388**, 149 (1997).

8) J. J. Napolitano, *et al.*, Nucl. Instrum. Methods A **274**, 152 (1989).
9) C. Athanassopoulos, *et al.*, Phys. Rev. C **55**, 2078 (1997).
10) E. Kolbe, K. Langanke, F.-K. Thielmann, and P. Vogel, Phys. Rev. C **52**, 3437 (1995).
11) B. Achkar, *et al.*, Nucl. Phys. **B434**, 503 (1995).
12) A. Romosan, *et al.*, Phys. Rev. Lett. **78**, 2912 (1997).
13) D. Autiero, talk presented at the 1998 International Conference on High Energy Physics in Vancouver, Canada.
14) K. Eitel, talk presented at the 2000 International Neutrino Conference in Sudbury, Canada.